Extreme Mechanics Letters 9 (2016) 282–290

Contents lists available at ScienceDirect

Extreme Mechanics Letters

journal homepage: www.elsevier.com/locate/eml

Elastic instabilities of a ferroelastomer beam for soft reconfigurable electronics

Vivek Ramachandran, Michael D. Bartlett, James Wissman, Carmel Majidi *

Department of Mechanical Engineering, Carnegie Mellon University, Pittsburgh 15213 PA, USA

ARTICLE INFO

Article history:
Received 14 December 2015
Received in revised form 5 August 2016
Accepted 5 August 2016
Available online 4 September 2016

Keywords:
Elastic instability
Ferromagnetic elastomer
Beam snapping
Soft-matter electronics

ABSTRACT

We examine the flexural deformation and snap-through instability of a pre-buckled ferroelastomer beam. The beam is composed of ferromagnetic and electrically conductive microparticles suspended in a polydimethylsiloxane (PDMS) matrix. Bending and snap-through are controlled remotely with an external magnetic field. The observed magneto-flexural coupling is in reasonable agreement with predictions from an analytic model based on elastic rod theory and variational techniques. Moreover, such coupling results in stable and unstable bending modes that can be exploited for a soft-matter, field-controlled, reconfigurable electrical relay. These two flexural modes correspond to (i) low-power binary (stable) switching and (ii) a more rapid >10 Hz response that is achieved by momentarily driving the beam to a slightly deformed configuration. This combination of stable and unstable switching states provides a new approach for harnessing elastic instabilities and a means to create a low power, yet rapidly responsive switch for soft electronic systems.

1. Introduction

Wearable computing and soft bio-inspired robotics depend on elastically deformable electronics that match the mechanical properties of natural biological tissue [1,2]. Stretchable circuit wiring and "artificial skin" sensing is currently accomplished with soft elastomer composites [3], soft microfluidics [4], and a variety of deterministic architectures involving wavy patterns and microscale geometries [5]. The latter approach typically exploits elastic instabilities such as buckling and wrinkling [1]. In addition to stretchable electronics, these elastic instabilities have also been used for adhesion and wetting control [6–8], shape-programmable origami [9,10], valves for manipulating fluid flow [11], reversible fluidic encapsulation [12], and elastocapillary snapping [13]. The dynamic loss of elastic stability and beam snapping has provided opportunities for pneumatic actuation [14], voltage-controlled dielectric elastomer actuators [15,16], and the control of optical properties through snapping microlens structures [17]. Moreover, buckling and snap-through govern dynamic elasto-morphological coupling in a variety of biological mechanisms. These include morphogenesis of the *Volvox* embryo [18], catapult-like ejection of fern sporangia [19], and the thigmonastic movement of the Venus flytrap (*Dionea* plants) [20]. For these engineered and biological systems, elastic instabilities have a central role in enabling stretchable functionality or reducing the energetic barrier for achieving dramatic changes in shape or morphology.

In this manuscript, we demonstrate the ability to exploit elastic instability for physically reconfigurable soft electronics. This is accomplished with a soft elastic switching element (Fig. 1(a)) that undergoes a buckling instability in response to an external magnetic field (Fig. 1(b); Movie S1 in SI). The switch is composed of a pre-buckled ferromagnetic elastomer beam that reversibly controls the electrical conductivity between a source and drain electrode. External magnetic field is used to induce either temporary deflection or snap-through between bistable states, allowing for two modes of

* Corresponding author.
E-mail address: cmajidi@andrew.cmu.edu (C. Majidi).
URL: http://sml.me.edu.cmu (C. Majidi).

http://dx.doi.org/10.1016/j.eml.2016.08.007
2352-4316/

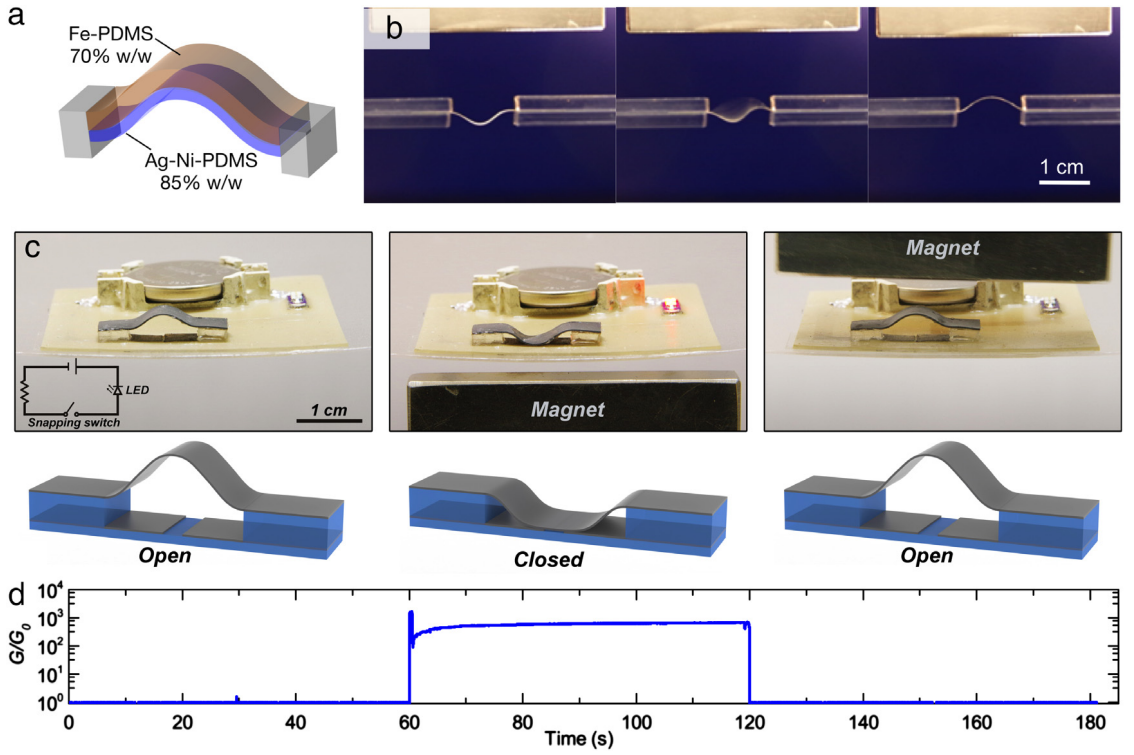

Fig. 1. (a) Model of the bilayered ferroelastomeric beam in a pre-buckled state (b) Doubly clamped bistable ferroelastic beam undergoing snap through (left to right) from one stable configuration to the other under the influence of an increasing external magnetic field (see Video S1 in the SI, Appendix A). (c) Demonstration of a soft, flexible switch by magnetically snapping a ferroelastomer beam (see Video S2, Appendix A) to open and close a circuit, as illustrated by turning on and off an LED. The schematics show the open and closed circuit states. (d) Normalized conductivity (G/G_0) of the circuit showing the change in electrical conductivity as the beam is snapped in and out of a closed configuration.

electrical switching behavior. We examine both through a combination of experimental observations and theoretical modeling based on elastic beam theory and variational techniques. The theory furnishes stability criteria that not only inform switch design but also allows us to predict the influence of subsequent stretch and external mechanical loading on switch response.

This work builds on previous studies on snap-through buckling instabilities [21–26] as well as the magneto-elastostatics of so-called magnetorheological (MR) elastomers. MR elastomers are composed of a dispersion of ferromagnetic microparticles (typically Fe, Ni, Co, or their alloys) suspended in an elastomeric matrix [27–31]. In this study, a prismatic strip of MR elastomer is coated with a layer of elastomer embedded with a percolating network of Ag-coated Ni microparticles. This conductive layer functions as a "gate" electrode that controls electrical connectivity between a pair of "source" and "drain" leads. The influences of composition on the magnetic, electrical, and mechanical properties of both the ferromagnetic and conductive elastomer composites are well understood [32–35]. There has also been growing interest in applying ferromagnetic elastomers for soft robotic sensing and actuation. This includes flexural elements for bending actuation, magnetically-powered origami, and a crawling soft robot cable of field-activated "self-locomotion" [36].

We begin by presenting the methods for fabricating an MR elastomer composite and field-activated switch in which the composite beam forms reversible electrical contact with a pair of source/drain leads (Fig. 1(c), (d); Movie S2). The leads are composed of liquid-phase eutectic gallium–indium (EGaIn) alloy sealed with an anisotropically conductive "z-film" elastomer that is only conductive through its thickness [37]. The response of the ferromagnetic beam to external magnetic field is found to be in reasonable agreement with theoretical predictions based on elastic rod theory and principle of minimum potential energy. In particular, the theory can be used to predict the proximity of the magnet at which snap-through instability occurs.

2. Experimental

The switching element shown in Fig. 1(a) is composed of two layers of elastomer composite. The top layer is a 80 μm thick strip of polydimethylsiloxane (PDMS) elastomer (Sylgard 184; 10:1 base-to-catalyst ratio; Dow Corning) embedded with 70% w/w Fe microparticles (spherical, diameter <10 μm; Alfa Aesar). The bottom layer is 30 μm thick and composed of PDMS embedded with 85% w/w Ag-coated Ni microparticles ($\sim$15 μm; Potters Industries). Both layers are prepared by shear mixing the uncured PDMS and microparticles with a stirring rod for 5 min. The Fe–PDMS layer is deposited using a thin-film applicator (ZUA 2000; Zehntner Testing Instruments). The elastomer is then partially cured at 70 °C for 20 min. Next, a layer of

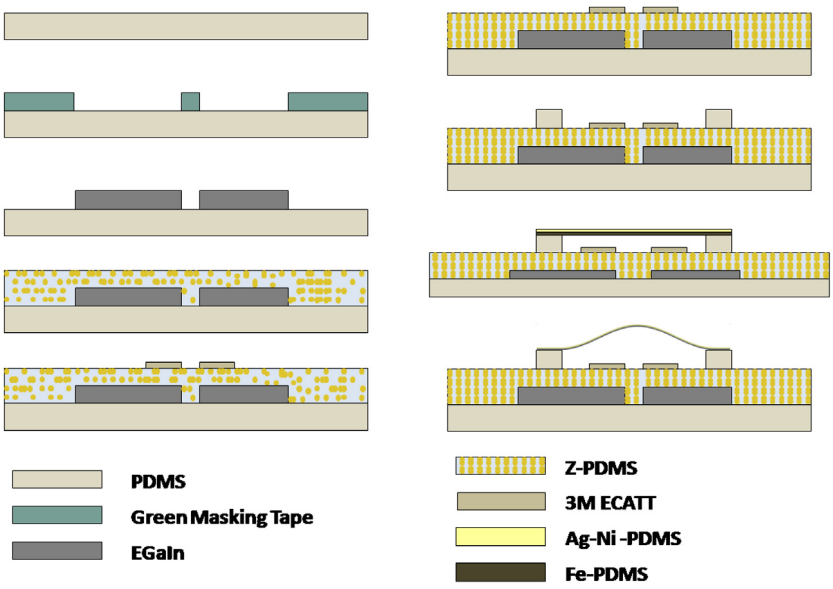

Fig. 2. Layup and fabrication method for the switch implementation. (For interpretation of the references to color in this figure legend, the reader is referred to the web version of this article.)

Ag–Ni–PDMS is deposited over the Fe–PDMS film and the composite is then fully cured at 70 °C for 90 min. The composite sheet is patterned into strips using a CO_2 laser (VLS 3.50; Universal Laser Systems). Each strip has total dimensions of $t = 110\ \mu m$ (thickness), $L_0 = 15.4$ mm (length), and $b = 5$ mm (width). It is assumed that the dispersion of the particles is random but statistically uniform throughout the volume. Both layers are ferromagnetic and only the Ag–Ni–PDMS layer is electrically conductive. The Fe–PDMS layer functions as the magnetically-powered actuator layer while the Ag–Ni–PDMS is used as the gate electrode for electrical switching.

2.1. Switch fabrication

The layup and fabrication method of the switch is presented in Fig. 2. First, we prepare a thin film substrate of PDMS (300 μm) and allow it to cure at 70 °C. Next, we lay down green masking tape (LaserTape; IKONICS Imaging Inc.) that is patterned with a CO_2 laser and deposit a thin film of liquid-phase eutectic gallium–indium alloy (EGaIn, 99.99% pure; Sigma–Aldrich). Removing the masking tape leaves behind 4 mm wide EGaIn traces that will function as a pair of source/drain electrodes. To prevent leakage, these liquid electrodes are sealed with a layer of Ag–Ni–PDMS conductive elastomer. Prior to curing, laser-patterned squares of conductive non-woven fabric (3M CN-3490) are placed on the surface of the elastomer, directly above the lead terminals. These will function as contact pads that make reversible electrical contact with the Ag–Ni–PDMS layer of the composite beam.

To prevent electrical conductivity between the elastomer-embedded EGaIn electrodes, a magnetic field is applied as the Ag–Ni–PDMS seal cures. This is accomplished by placing the sample above a permanent magnet (NdFeB; K&J Magnetics, Inc.) while it cures in an oven for 45 min at 70 °C. The magnetic field causes the Ag-coated Ni particles to self-assemble into vertically aligned columns. This results in an anisotropically conductive "z-film" elastomer that is only conductive through its thickness ($\mathbf{e}_z$). A coin cell battery holder (BU2032SM-HD-G, Digi-Key Electronics Inc.) and LED (DEV-10754 ROHS, Lily-Pad LED Micro—Red, Sparkfun Inc.) is mounted to the surface of the Ag–Ni–PDMS seal during curing. After the seal is cured, the substrate is stretched and bonded to the ferroelastomer switch. The switch itself is composed of the ferroelastomer strip supported by two vertical PDMS posts. The posts are bonded to the pre-stretched substrate using a silicone adhesive (Sil-Poxy; Smooth-On Inc.). Once the beam is bonded firmly onto the posts, the substrate is released and the beam undergoes compression and buckling.

2.2. Critical magnet distance for snap-through

Snap through occurs when the vertical distance d between the supports of the ferroelastic beam and the surface of an external magnet ($2'' \times 2'' \times 1/4''$ NdFeB magnet; K&J Magnetics, Inc.) reaches a critical value d_{cr}. This critical separation is determined by vertically lowering the magnet towards the beam, which is initially buckled away from it. The magnet is mounted on to the travel head of a materials testing system (Instron 5969) and is lowered at a rate of 10 mm/min. The d_{cr} values are measured from a video analysis and modeling software (Tracker, Inc.) of video recordings of the beam as it transitions from one stable state to the other.

3. Principles & theory

The snap-through instability demonstrated in Fig. 1 can be explained by an analytic model based on elastic rod theory and the principal of minimum potential. Referring

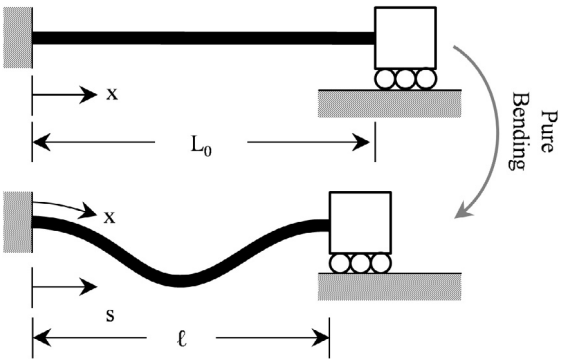

Fig. 3. Beam deformation is described by pure bending.

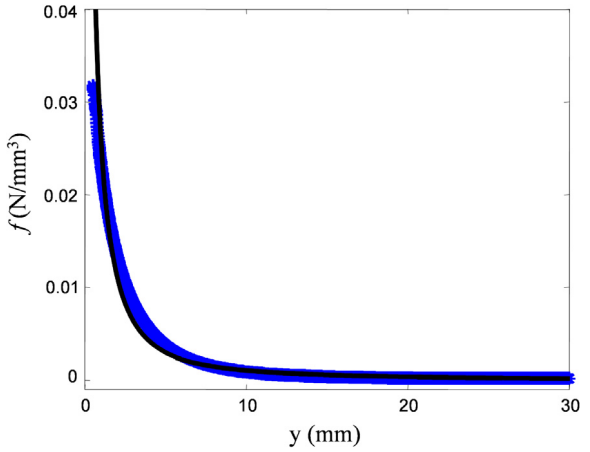

Fig. 4. Variation in the magnetic force density f of the permanent magnet with vertical distance y from the testing face to the point of measurement, $\beta = 822.6$ is the fitting parameter.

to Fig. 3, the beam is initially straight with the supports separated by the natural length L_0 of the beam. Next, the separation is reduced to $\ell < L_0$, which causes the beam to compress and buckle. From this pre-buckled reference state, the deflection of the beam is controlled with an external force-inducing field (e.g. gravitational, magnetic, electrostatic). At each point in the beam, this field exerts a force density $\mathbf{f} = f\mathbf{e}_z$, where $\mathbf{e}_z$ is the unit vector along the beam's minor axis and f has units of N/mm^3. When the field source is located at a nominal distance y above the supports, the force density is expected to scale with y^n, i.e. $f = \beta y^n$, where β is a fitting parameter associated with the choice of the field source. In this study, a magnet is centered a distance d above the beam supports, has a N/S orientation aligned with the beam's minor axis ($\mathbf{e}_z$), and the force density is measured to scale as $y^{-3/2}$ (Fig. 4; see also Sec. S1 in the SI).

3.1. Kinematics

Prior to buckling, the beam has a natural length L_0, width b, thickness t, and cross-sectional area $A_0 = bt$. The variable $x \in [0, L_0]$ represents the axial coordinate in the Lagrangian (natural, undeformed) description. Although the beam is composed of two layers, it is convenient to treat it as a uniform elastic rod with uniform density ρ, Young's modulus E, and flexural rigidity $D = Ebt^3/12$. Referring to Fig. 3, beam deformation is described by pure bending, during which the arclength L_0 remains fixed and cross-sectional elements along the beam have a vertical deflection $w = w(x)$. For a given end-to-end separation ℓ, it is convenient to define a horizontal stretch $\hat{\lambda} := \ell/L_0$. In this way, $\hat{\lambda}$ and $w(x)$ can be related by the following isoperimetric constraint:

$$\hat{\lambda} = \frac{\ell}{L_0} = \frac{1}{L_0}\int_0^{L_0} \sqrt{1 - w_{,x}^2}\, dx\,. \tag{1}$$

The clamped–clamped supports also prevent vertical displacement and rotation at the ends:

$$w(0) = w_{,x}(0) = w(\ell) = w_{,x}(\ell) = 0. \tag{2}$$

The subscript $_{,x}$ denotes the derivative w.r.t. the coordinate x.

We restrict w to approximations of the form $w \approx \alpha_1\phi_1 + \alpha_2\phi_2$. Here, $\{\phi_1, \phi_2\}$ are linearly independent basis functions and $\{\alpha_1, \alpha_2\}$ are the corresponding weighting coefficients. For the basis functions, we selected mode shapes that are in qualitative agreement with experimentally observed deflections (see Sec. S2 of the SI):

$$\phi_1 = \frac{1}{2}\left\{1 - \cos\left(\frac{2\pi x}{L_0}\right)\right\}, \tag{3}$$

$$\phi_2 = \frac{4}{3\sqrt{3}}\sin\left(\frac{2\pi x}{L_0}\right)\left\{1 - \cos\left(\frac{2\pi x}{L_0}\right)\right\}. \tag{4}$$

Substituting this approximation for w into (1) yields a relationship between the unknown coefficients α_1 and α_2.

3.2. Potential energy

In general, the load per unit length (f_t) and total potentially energy (U) associated with the external force-inducing fields have the form

$$f_t = \sum_\xi q_\xi (d - w)^{p_\xi}, \tag{5}$$

$$U = \sum_\xi \int_0^{L_0} \frac{q_\xi}{p_\xi + 1}(d - w)^{p_\xi + 1} dx. \tag{6}$$

Here, q_ξ is the coefficient of the field load which is dependent on the flexural and material properties of the beam, d is the distance between the source of the field and the beam mid-plane, and p_ξ describes the dependency between the force density and the distance between the source and each point on the beam. For our system, the beam is subject to only gravitational and magnetic loading. The coefficient of the gravitational load can be represented as $q_g = \rho A_0 g$, where $\rho = k\rho_m + (1 - k)\rho_e$ is the average specific density of the composite and g is the gravitational acceleration. Here, k is the mass fraction of the ferromagnetic particles and ρ_m and ρ_e are the specific density of the particles and elastomer, respectively. The coefficient of the magnetic load is defined as $q_m = \beta A_0$, which is independent of the beam deflection. For the

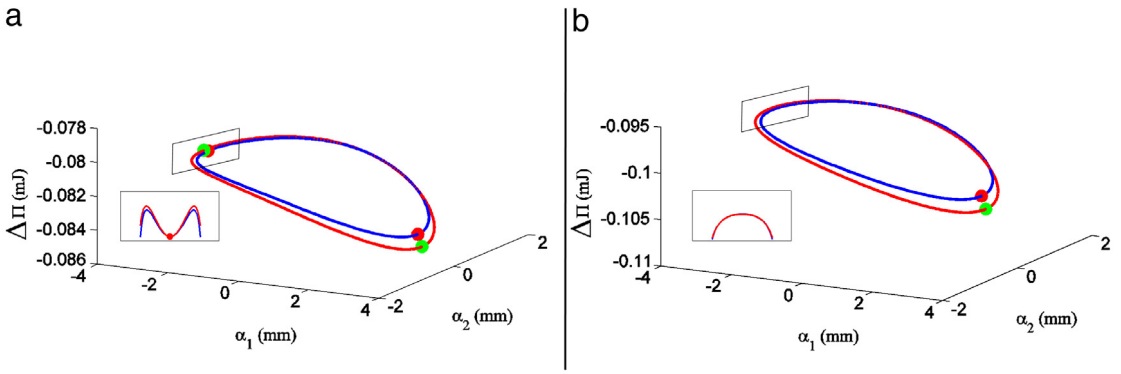

Fig. 5. Numerical (blue) and analytical (red) results for the relative variation in the potential energy along the "valley" under (a) sub-critical magnetic load ($d = 21$ mm) and (b) post-critical magnetic load ($d = 30$ mm), with local and global minima indicated (numerical (red dot) and analytical (green dot)). The value of the coefficient of magnetic load is $q_m = 0.452$ mN m$^{1/2}$. (For interpretation of the references to color in this figure legend, the reader is referred to the web version of this article.)

gravitational load and the magnetic load, the values of p_g and p_m are 0 and $-3/2$, respectively.

At static equilibrium, the elastic deformation of the beam is determined by extremizing the total potential energy functional $\Pi = \Pi(\lambda, w)$. The potential Π is composed of the elastic strain energy (from bending), and the energy associated with gravity and magnetic field.

$$\Pi = \int_0^{L_0} \left\{ \frac{1}{2} D w_{,xx}^2 + q_g w - \frac{2q_m}{(d-w)^{1/2}} \right\} dx. \tag{7}$$

To obtain an approximate solution for w, we first apply the isoperimetric constraint in order to eliminate α_1 and express w and Π only in terms of α_2. Next we determine the value of α_2 at which Π is stationary (i.e. $\mathrm{d}\Pi/\mathrm{d}\alpha_2 = 0$). Lastly, we compute the second variation $\mathrm{d}^2\Pi/\mathrm{d}\alpha_2^2$ to determine whether the solution is stable (i.e. Π is locally minimized). Numerical solutions are obtained in MATLAB (R2015a; The Mathworks, Inc.) and an analytic approximation is obtained by performing Taylor series expansions on (1) and (7).

3.3. Approximation

To obtain an approximate scalar function for the potential $\Pi \approx \Pi(\alpha_1, \alpha_2)$, we substitute the expression for $w = w(\alpha_1, \alpha_2)$ into (7) and perform a Taylor series expansion (see Sec. S2):

$$\begin{aligned}\Pi \approx{}& \frac{D\pi^4}{L_0^3}\left(\alpha_1^2 + \frac{320}{27}\alpha_2^2\right) + \frac{L_0 q_g \alpha_1}{2} \\ &- \frac{L_0 q_m}{d^{3/2}}\left\{\frac{\alpha_1}{2} + \frac{1}{228d}\left(81\alpha_1^2 + 80\alpha_2^2\right)\right. \\ &\left. + \frac{5\alpha_1}{1152d^2}\left(45\alpha_1^2 + 112\alpha_2^2\right)\right\}. \end{aligned} \tag{8}$$

Next, α_1 is estimated from a Taylor series approximation of the unilateral constraint (1):

$$\tilde{\alpha}_1 = \pm\left\{\left(\frac{L_0}{\pi}\right)^2 (1-\hat{\lambda}) - \frac{32}{27}\alpha_2^2\right\}^{1/2}. \tag{9}$$

For our analysis, the beam is initially buckled away from the source of the magnetic field and therefore, we consider the beam to have a negative value of $\tilde{\alpha}_1$.

Substituting (9) in (8), we obtain $\Pi = \tilde{\Pi}(\alpha_2)$, which must be locally convex at stable equilibrium. In the absence of magnetic and gravitational load, $d^2\tilde{\Pi}^*/d\alpha_2^2 \approx 128\pi^4 EI/9L_0^3 > 0$, which implies that the buckled shape $\alpha_1 = \tilde{\alpha}_1$, $\alpha_2 = 0$ is elastically stable. However, applying an increasing magnetic loading in the direction opposite of the deflection will cause the second variation to decrease until the stability criterion is no longer satisfied. Of particular interest is the critical separation of the magnet from the midplane (d_{cr}) at which snap-through occurs. This is obtained by finding the solution of d to the condition $d^2\tilde{\Pi}^*/d\alpha_2^2 = 0$:

$$\begin{aligned}&-\frac{32\pi}{27}\frac{q_m}{d^{3/2}}(1-\hat{\lambda})^{-1/2} + \frac{19}{9}\frac{q_m}{d^{3/2}}\frac{L_0}{d} \\ &-\frac{65}{18}\frac{q_m}{\pi d^{3/2}}\left(\frac{L_0}{d}\right)^2(1-\hat{\lambda})^{1/2} \\ &+\frac{32}{27}\frac{Ebt^3\pi^4}{L_0^3} + \frac{32\pi}{27}q_g(1-\hat{\lambda})^{-1/2} = 0. \end{aligned} \tag{10}$$

4. Results

To understand the behavior of the bistable beam as it changes configuration from one stable state to the other after undergoing snap-through, it helps to examine the following cases separately: (i) deflection under low magnetic loading, and (ii) snap-through instability. For this analysis (see Fig. 5), we used the following system parameters: $\rho_m = 8000$ kg m^{-3}, $\rho_e = 965$ kg m^{-3}, $k = 0.8$, $E = 6.0$ MPa, $\beta = 822.6$ N m$^{3/2}$, $q_m = 0.452$ mN m$^{1/2}$, $L_0 = 15.4$ mm, $b = 5$ mm, $t = 110$ μm, and $\hat{\lambda} = 0.9$. In Fig. 5, the curve corresponding to the numerical solution was generated by solving (1) in MATLAB (R2013a; The Mathworks, Inc.) using the native *integral* and *fsolve* functions. In contrast, the curve corresponding to the analytical solution was generated from the approximation for α_1 given in (9). Corresponding values for q_m and d are provided in the figure caption.

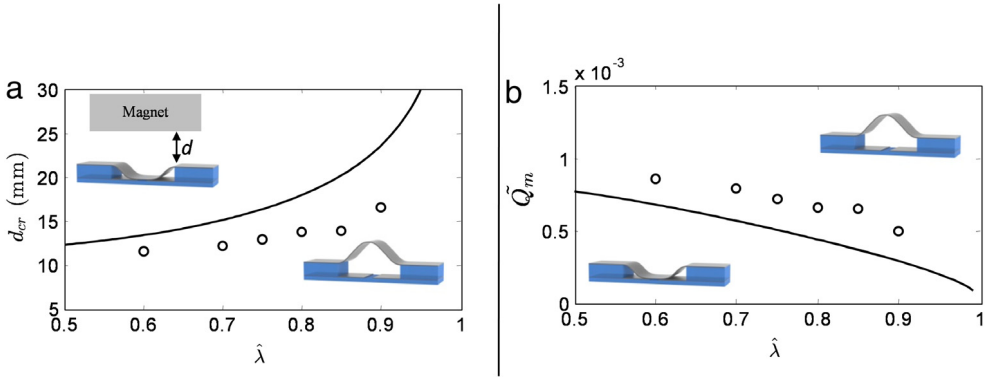

Fig. 6. (a) Critical distance d_{cr} versus $\hat{\lambda} = \ell/L_0$ and (b) critical non-dimensional magnetic loading $\tilde{Q}_m := q_m L_0/EA_0 {d_{\mathrm{cr}}}^{3/2}$ versus $\hat{\lambda} = \ell/L_0$ for the analytical model (solid) and experimental calculations (markers). As the magnet approaches the downward deflected beam, d_{cr} corresponds to the critical distance at which snap-through is induced. At this critical distance, $\tilde{Q}_m$ corresponds to the normalized load exerted on the beam. As expected, d_{cr} decreases and $\tilde{Q}_m$ increases, respectively, as the resistance to snap-through increases with increasing pre-buckled deflection (i.e. decreasing $\hat{\lambda}$).

4.1. Sub-critical load

Prior to introducing the magnet, the beam is observed to either deflect up or down and adopt the first mode shape ϕ_1 (i.e. $\alpha_2 = 0$). This corresponds to the conventional bifurcation instability associated with compressive preload and buckling. Next, suppose that a magnet is placed on the side opposite the direction of deflection. According to the approximate theory the beam will not deflect from its pre-buckled state so long as $d > d_{\mathrm{cr}}$. However, in practice we observe a modest decrease in amplitude $|\alpha_1|$ due to the elastic compressibility of the magnetically loaded beam. Such deformation is reversible and the beam will spring back to its original deflection when the magnet is removed. As described below in Section 4.3, this sub-critical loading can be exploited for a high frequency relay in which electrical contact between the source/drain electrodes is only temporarily broken when a magnet is applied. It is important to recognize that for such applications, the theory will need to be modified to account for the unilateral contact with the electrodes.

4.2. Post-critical load

Again suppose that the beam is initially deflected away from the magnet. As the magnet is brought closer to the beam, d will eventually reach the critical separation d_{cr} necessary to induce a snap-through instability. During snap-through, α_2 becomes non-zero and the beam exhibits a linear combination of the first and second bending modes. Referring to Fig. 5(b), these transitional values of α_1 and α_2 correspond to the path along which the decrease in Π is steepest. An analogous behavior is observed in the study of diatomic molecules, where such a transition is referred to as the lowest-energy pathway or intrinsic reaction coordinate (IRC) curve [38]. These correspond to physical "transition states" or configurations that the momentarily beam adopts as it approaches its stable state.

Fig. 6(a) shows the dependency of d_{cr} on $\hat{\lambda} = \ell/L_0$ for the analytical model. Greater axial compression (lower $\hat{\lambda}$) results in a greater initial downward deflection and larger mechanical resistance to snap-through. Therefore, the magnet must be in closer proximity to the beam in order to generate the magnetic load necessary to induce the instability. Another way to examine this is the change in magnitude of the corresponding critical magnetic load, $\tilde{Q}_m$, which is non-dimensionalized with respect to flexural rigidity and d_{cr}:

$$\tilde{Q}_m := \frac{q_m L_0}{EA_0 d_{\mathrm{cr}}^{3/2}}. \tag{11}$$

For given beam dimensions (L_0, A_0), elastic modulus E, and magnet distance d, it follows that stretching the beam from its buckled state (thereby decreasing the compression and consequently, increasing $\hat{\lambda}$) reduces the magnetic load required to induce snap-through instability. Also, a more rigid beam (i.e. larger EA_0/L_0) will require a greater nominal load $q_m/d_{\mathrm{cr}}^{3/2}$. This is consistent with the intuition that a larger initial deflection away from the magnet and greater flexural rigidity of the beam will both increase resistance to snap through. As shown in Fig. 6(b), the curve intersects the x-axis at $\hat{\lambda} = 1$. This arises from the assumption that the rod is inextensible/incompressible and only undergoes flexural deformation.

4.3. Switch implementation

A principle feature of the pre-buckled ferroelastomer switch is its ability to exhibit either reversible or snap-through responses when subject to magnetic loading (Fig. 7(a)). When snapping between the two stable configurations, we demonstrate the ability to reversibly switch between closed and open circuit states. In this case, the magnetic field is only necessary for switching. However, when a low oscillatory magnetic field is applied, the beam exhibits temporary and reversible deformation. In this case, removing the field causes the beam to spring back to its original deflection. This response corresponds to a higher frequency switching mode that rapidly oscillates between an open and closed circuit. This fast switching behavior is demonstrated in Fig. 7(b), where the switch is activated with a sub-critical magnetic field. After one second of reversible switching, the magnetic field is

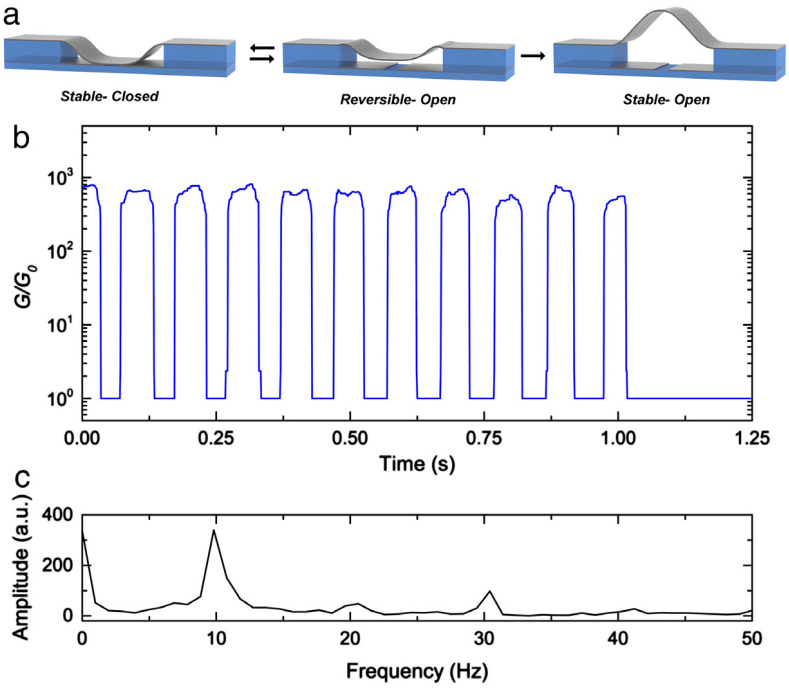

Fig. 7. (a) Schematic representation of the three states during fast switching. (b) Experimental data showing fast switching between the stable-closed and reversible-open states for 1 s followed by a snap through transition to the stable-open configuration. (c) FFT of the data in part b showing the strong peak at 10 Hz switching frequency.

increased such that $d < d_{cr}$. This causes snap-through to the permanently open circuit. By taking a Fast Fourier Transform (FFT) of the conductivity data (Fig. 7(c)), we see a strong peak at 10 Hz, which we designate as the primary switching frequency. This frequency was limited by our experimental setup, and further investigated into the limits of the high frequency switching could be explored by varying geometry and material parameters.

5. Discussion

In this work, we demonstrate an implementation of a switching element in a flexible circuit by utilizing the buckling instabilities of a bistable ferroelastomer beam. For a given set of material and dimensional properties, the behavior of the beam is studied for a variety of magnetic loading conditions. Depending upon the operational requirements of the switch, there are certain considerations that need to be accounted for while designing and fabricating the beam for the switching element. For example, the elastic modulus E of the beam is influenced by the volume fraction of rigid microparticles and the modulus of the elastomer matrix. In particular, it follows from (10) that d_{cr} decreases with modulus. This is consistent with physical observation—more rigid beams are more resistant to snap-through instability.

It is also expected that as $\hat{\lambda}$ decreases, the amount of magnetic load required to induce snap-through also increases for the same nominal gap. This is supported by the experimental results shown in Fig. 6 and suggests that a switch will become less resistant to snap-through as the buckling induced compression is reduced. When the non-dimensional magnetic load exceeds $\tilde{Q}_m$, the beam will undergo snap-through. Below this value, the deflection is reversible, i.e. the beam will return to its original shape when the magnetic field is removed. This has important implications when selecting thresholds for the magnetic loads used to excite reversible and permanent switching responses.

The pre-buckled ferroelastomer beam bears some resemblance to switch designs used in the microelectromechanical systems (MEMS). In MEMS, actuation schemes can broadly be classified into the following categories: electrostatic, piezoelectric, thermomechanical, and electromagnetic. Despite its immense popularity and low power consumption, electrostatic actuation requires high pull-in voltages and generally results in small displacements. Alternatively, thermomechanical loading is capable of generating large displacements with high forces, but its power requirements are correspondingly large for slow response rates. Piezoelectric actuation is promising but required rigid materials that are no capable of being stretchable. In contrast, electromagnetic actuators are capable of rapidly producing adequate forces and displacements with relatively low mechanical work input and can be produced with soft materials. Here, we show that such low power functionality can be accomplished with bistability and the use of a permanent magnet.

6. Conclusion

We have introduced a soft reconfigurable electrical contact that utilizes magneto-flexural coupling and snap-through instability. This switch is composed of a pre-buckled ferroelastomer strip that deforms in response

to an external magnetic field. It exploits snap-through mechanics in order to transition between an open and closed-circuit configuration. For low magnetic loads, there is a second switching mode—the circuit is only temporarily opened when field is applied and returns to being closed when field is removed. The switch response is explained with an analytic model derived by applying the Rayleigh–Ritz method to examine the static equilibrium of a ferromagnetic elastic rod. A key result of this analysis is a stability criterion that relates a non-dimensional critical magnetic load for snap-through $\tilde{Q}_m$ with the ratio $\hat{\lambda} = \ell/L_0$ of the support separation and beam length.

Acknowledgments

The authors wish to thank Tong Lu (Soft Machines Lab; CMU) with assistance in selecting a composition for the anisotropically conductive "z-PDMS" film. This work was partially supported by a NASA Early Career Faculty Award (Grant #NNX14AO49G) and ONR Young Investigator Award (Grant #N000141210614; Code 34; PM: Dr. Tom McKenna).

Appendix A. Supplementary data

This manuscript is accompanied with details of the method for measuring magnetic field and fabricating the electrical switch. Videos showing the snap-through instability and switch response are also include.

Supplementary material related to this article can be found online at http://dx.doi.org/10.1016/j.eml.2016.08.007.

References

[1] J.A. Rogers, T. Someya, Y. Huang, Materials and mechanics for stretchable electronics, Science 327 (5973) (2010) 1603–1607. http://dx.doi.org/10.1126/science.1182383, URL http://www.ncbi.nlm.nih.gov/pubmed/20339064.

[2] C. Majidi, Soft robotics: A perspective - current trends and prospects for the future, Soft Robot. 1 (1) (2014) 5–11.

[3] H.-J. Koo, J.-H. So, M.D. Dickey, O.D. Velev, Towards all-soft matter circuits: prototypes of quasi-liquid devices with memristor characteristics, Adv. Mater. 23 (31) (2011) 3559–3564. http://dx.doi.org/10.1002/adma.201101257, URL http://www.ncbi.nlm.nih.gov/pubmed/21726000.

[4] H.-J. Kim, C. Son, B. Ziaie, A multiaxial stretchable interconnect using liquid-alloy-filled elastomeric microchannels, Appl. Phys. Lett. 92 (1) (2008) 011904. http://dx.doi.org/10.1063/1.2829595, URL http://scitation.aip.org/content/aip/journal/apl/92/1/10.1063/1.2829595.

[5] D.-H. Kim, N. Lu, R. Ma, Y.-S. Kim, R.-H. Kim, S. Wang, J. Wu, S.M. Won, H. Tao, A. Islam, et al., Epidermal electronics, Science 333 (6044) (2011) 838–843.

[6] E.P. Chan, E.J. Smith, R.C. Hayward, A.J. Crosby, Surface wrinkles for smart adhesion, Adv. Mater. 20 (4) (2008) 711–716. http://dx.doi.org/10.1002/adma.200701530.

[7] D.R. Paretkar, M.D. Bartlett, R. McMeeking, A.J. Crosby, E. Arzt, Buckling of an adhesive polymeric micropillar, J. Adhes. 89 (2) (2013) 140–158. http://dx.doi.org/10.1080/00218464.2013.731941, URL http://www.tandfonline.com/doi/abs/10.1080/00218464.2013.731941.

[8] J.Y. Chung, J.P. Youngblood, C.M. Stafford, Anisotropic wetting on tunable micro-wrinkled surfaces, Soft Matter 3 (9) (2007) 1163. http://dx.doi.org/10.1039/b705112c.

[9] Z. Chen, Q. Guo, C. Majidi, W. Chen, D.J. Srolovitz, M.P. Haataja, Nonlinear geometric effects in mechanical bistable morphing structures, Phys. Rev. Lett. 109 (11) (2012) 114302. URL http://dx.doi.org/10.1103/PhysRevLett.109.114302.

[10] N.P. Bende, A.A. Evans, S. Innes-Gold, L.A. Marin, I. Cohen, R.C. Hayward, C.D. Santangelo, Geometrically controlled snapping transitions in shells with curved creases, Proc. Natl. Acad. Sci. USA 112 (36) (2015) 11175–11180. URL www.pnas.org/cgi/doi/10.1073/pnas.1509228112.

[11] D.P. Holmes, B. Tavakol, G. Froehlicher, H.a. Stone, Control and manipulation of microfluidic flow via elastic deformations, Soft Matter 9 (29) (2013) 7049. http://dx.doi.org/10.1039/c3sm51002f, URL http://xlink.rsc.org/?DOI=c3sm51002f.

[12] J. Shim, C. Perdigou, E.R. Chen, K. Bertoldi, P.M. Reis, Buckling-induced encapsulation of structured elastic shells under pressure, Proc. Natl. Acad. Sci. 109 (16) (2012) 5978–5983. http://dx.doi.org/10.1073/pnas.1115674109.

[13] A. Fargette, S. Neukirch, A. Antkowiak, Elastocapillary snapping: Capillarity induces snap-through instabilities in small elastic beams, Phys. Rev. Lett. 112 (13) (2014) 137802. URL http://dx.doi.org/10.1103/PhysRevLett.112.137802.

[14] J.T.B. Overvelde, T. Kloek, J.J.A. Dhaen, K. Bertoldi, Amplifying the response of soft actuators by harnessing snap-through instabilities, Proc. Natl. Acad. Sci. 112 (35) (2015) 10863–10868. http://dx.doi.org/10.1073/pnas.1504947112.

[15] C. Keplinger, T. Li, R. Baumgartner, Z. Suo, S. Bauer, Harnessing snap-through instability in soft dielectrics to achieve giant voltage-triggered deformation, Soft Matter 8 (2) (2012) 285. http://dx.doi.org/10.1039/c1sm06736b, URL http://xlink.rsc.org/?DOI=c1sm06736b.

[16] J. Wissman, L. Finkenauer, L. Deseri, C. Majidi, Saddle-like deformation in a dielectric elastomer actuator embedded with liquid-phase gallium-indium electrodes, J. Appl. Phys. 116 (14) (2014) 144905. URL http://dx.doi.org/10.1063/1.4897551.

[17] D.P. Holmes, A.J. Crosby, Snapping surfaces, Adv. Mater. 19 (2007) 3589–3593. http://dx.doi.org/10.1002/adma.200700584, URL http://scholar.google.com/scholar?hl=en&btnG=Search&q=intitle:Snapping+Surfaces#0.

[18] S. Hhn, A.R. Honerkamp-Smith, P.A. Haas, P. Khuc Trong, R.E. Goldstein, Dynamics of a volvox embryo turning itself inside out, Phys. Rev. Lett. 114 (17) (2015) 178101. URL http://dx.doi.org/10.1103/PhysRevLett.114.178101.

[19] X. Noblin, N.O. Rojas, J. Westbrook, M. Llorens, C. Argentina, J. Dumais, The fern sporangium: A unique catapult, Science 335 (110) (2012) 6074. URL http://dx.doi.org/10.1126/science.1215985.

[20] Q. Guo, E. Dai, X. Han, S. Xie, E. Chao, Z. Chen, Fast nastic motion of plants and bio-inspired structures, J. R. Soc. Interface 12 (110) (2015) 20150598. URL http://dx.doi.org/10.1098/rsif.2015.0598.

[21] P. Seunghoon, H. Dooyoung, Pre-shaped buckled-beam actuators: Theory and experiments, Sensors Actuators A 148 (2008) 186–192. http://dx.doi.org/10.1016/j.sna.2008.07.009.

[22] E. Dowell, Comment on "On dynamic snap buckling of shallow arches", AIAA J. 4 (5) (1966) 1887–1888. http://dx.doi.org/10.2514/3.55295.

[23] J. Zhao, J. Jia, X. He, H. Wang, Post-buckling and snap-through behavior of inclined slender beams, J. Appl. Mech. 75 (July) (2008) 041020. http://dx.doi.org/10.1115/1.2870953.

[24] M. Vangbo, Y. Bäcklund, A lateral symmetrically bistable buckled beam, J. Micromech. Microeng. 8 (1999) 29–32. http://dx.doi.org/10.1088/0960-1317/8/1/005.

[25] M. Vangbo, An analytical analysis of a compressed bistable buckled beam, Sensors Actuators A 69 (98) (1998) 212–216. http://dx.doi.org/10.1016/S0924-4247(98)00097-1.

[26] L. Medina, R. Gilat, S. Krylov, Symmetry breaking criteria in electrostatically loaded bistable curved/prebuckled micro beams, Progress Opt. Sci., Photonics (July) (2013) 679–705. http://dx.doi.org/10.1007/10091, arXiv:1403.7130 URL http://arxiv.org/abs/1403.7130.

[27] Y. Shen, M.F. Golnaraghi, G.R. Heppler, Experimental research and modeling of magnetorheological elastomers, J. Intell. Mater. Syst. Struct. 15 (1) (2004) 27–35. http://dx.doi.org/10.1177/1045389X04039264, arXiv:http://jim.sagepub.com/content/15/1/27.full.pdf+html URL http://jim.sagepub.com/content/15/1/27.abstract.

[28] M. Yalcintas, H. Dai, Magnetorheological and electrorheological materials in adaptive structures and their performance comparison, Smart Mater. Struct. 8 (5) (1999) 560. URL http://stacks.iop.org/0964-1726/8/i=5/a=306.

[29] G. Stepanov, S. Abramchuk, D. Grishin, L. Nikitin, E.Y. Kramarenko, A. Khokhlov, Effect of a homogeneous magnetic field on the viscoelastic behavior of magnetic elastomers, Polymer 48 (2) (2007) 488–495.

[30] W. Miles, J. Goff, P. Huffstetler, O. Mefford, J. Riffle, R. Davis, The design of well-defined pdms–magnetite complexes, Polymer 51 (2) (2010) 482–491.

[31] B.A. Evans, B.L. Fiser, W.J. Prins, D.J. Rapp, A.R. Shields, D.R. Glass, R. Superfine, A highly tunable silicone-based magnetic elastomer with nanoscale homogeneity, J. Magn. Magn. Mater. 324 (4) (2012) 501–507.
[32] J.D. Carlson, M.R. Jolly, Mr fluid, foam and elastomer devices, Mechatronics 10 (4) (2000) 555–569.
[33] J.M. Ginder, M.E. Nichols, L.D. Elie, J.L. Tardiff, Magnetorheological elastomers: properties and applications, in: 1999 Symposium on Smart Structures and Materials, International Society for Optics and Photonics, 1999, pp. 131–138.
[34] J.M. Ginder, M.E. Nichols, L.D. Elie, S.M. Clark, Controllable-stiffness components based on magnetorheological elastomers, in: SPIE's 7th Annual International Symposium on Smart Structures and Materials, International Society for Optics and Photonics, 2000, pp. 418–425.
[35] S. Abramchuk, D. Grishin, E.Y. Kramarenko, G. Stepanov, A. Khokhlov, Effect of a homogeneous magnetic field on the mechanical behavior of soft magnetic elastomers under compression, Polym. Sci. Ser. A 48 (2) (2006) 138–145.
[36] S. Ahmed, C. Lauff, A. Crivaro, K. McGough, R. Sheridan, M. Frecker, P. von Lockette, Z. Ounaies, T. Simpson, J.-M. Lien, R. Strzelec, Multi-field responsive origami structures: Preliminary modeling and experiments, in: Proc. ASME IDETC/CIE 6B (DETC2013) (2013) V06BT07A028. http://dx.doi.org/10.1115/DETC2013-12405.
[37] T. Lu, J. Wissman, Ruthika, C. Majidi, Soft anisotropic conductors as electric vias for ga-based liquid metal circuits, ACS Appl. Mater. Interfaces 7 (48) (2015) 26923–26929.
[38] K. Fukui, The path of chemical reactions-the irc approach, Acc. Chem. Res. 14 (12) (1981) 363–368.